Performance of the Multibeam Satellite Return Link with Correlated Rain Attenuation

Jesús Arnau, *Student Member, IEEE,* Dimitrios Christopoulos, *Student Member, IEEE,* Symeon Chatzinotas, *Senior Member, IEEE,* Carlos Mosquera, *Senior Member, IEEE* and Björn Ottersten, *Fellow, IEEE*

Abstract—Rain attenuation is among the major impairments for satellite systems operating in the K band and above. In this paper, we investigate the impact of spatially correlated rain attenuation on the performance of a multibeam satellite return link. For a comprehensive assessment, an analytical model for the antenna pattern that generates the beams is also proposed. We focus on the *outage capacity* of the link, and obtain analytical approximations at high and low SNR. The derived approximations provide insights on the effect of key system parameters – like the inter-user distance, the satellite beam radius, or the rain intensity– and simulation results show that it fits tightly to the Monte Carlo results. Additionally, the derived expressions can be easily particularized for the single-user case, providing some novel insights.

Index Terms—Multibeam satellites, rain attenuation, satellite communications, return link.

I. INTRODUCTION

Rain attenuation is known to be one of the major impairments of satellite and terrestrial communications in bands above 10 GHz [2]. These links' capacity [3] has been exploited in many ways, but adaptive coding and modulation (ACM) has proven to be the most efficient one.

Such capacity is becoming increasingly valuable: as increasing volumes of multimedia contents are demanded through satellite links, higher throughput and improved availability are being sought, shifting the payload to higher bands, exploiting multibeam coverages, and even envisaging joint multi-user processing [4]–[9].

So far, studies on the performance of such systems have assumed uncorrelated rain attenuation among different beams [4], [5], which is considered to be accurate for large beam diameters [4], [10]. However, spatial correlation of rain attenuation is known to degrade performance of other wireless systems, both satellite and terrestrial. In satellite communications, its impact has been widely studied in the context of site diversity [11]–[13] and SIMO and MISO broadband transmission [14]. For terrestrial applications, available studies include dual-hop relay systems [15], MIMO broadband communications [16] and cellular systems [17].

J. Arnau and C. Mosquera are with the Signal Theory and Communications Department, University of Vigo, Spain. C. Mosquera is also with the Galician Research and Development Center in Advanced Telecommunications (GRADIANT), Vigo, Spain. Email: {suso,mosquera}@gts.uvigo.es.

D. Christopoulos, S. Chatzinotas and B. Ottersten are with the SnT-University of Luxembourg. Email: {dimitrios.christopoulos,Symeon.Chatzinotas,bjorn.ottersten}@uni.lu.

Part of this work was presented at the 6th Advan. Satell. Multimedia Sys. Conf. (ASMS 2012), Baiona, Spain [1].

In this paper, we study the impact of spatially correlated rain attenuation over a multibeam satellite return link with full frequency reuse –all the beams using the same frequency band. For a comprehensive assessment, we start by proposing an analytical model for the antenna pattern that generates the beams. Then, we briefly study the *ergodic capacity* of the link, showing that, at high signal-to-noise ratio (SNR), the loss induced by rain tends to be constant, that is, independent of the SNR value and dependent only on the rain statistics. Ergodic capacity represents the maximum rate achievable with arbitrarily low error probability as long as we can code over a sufficiently large number of channel realizations.

However, this is not the case of rain-faded satellite links, because codewords usually span only a few realizations of the channel, a situation commonly known as *slow fading*; as an example, [18, Eq. 11] suggests rain fading coherence times of hundreds of seconds. In this case, ergodic capacity represents the average rate at which we can transmit with perfect channel state information (CSI) at the transmitter.

For this reason, in this paper we focus on the *outage capacity* of the link, which is the maximum transmission rate at which the outage probability does not exceed a given value ϵ. We derive high and low SNR approximations that provide insights on the effect of key system parameters – like the inter-user distance, the satellite beam radius, or the rain intensity. Analytical results are verified through extensive Monte Carlo simulations. Additionally, the derived expressions can be easily particularized for the single-user case, providing some novel insights; note that the single-user case is relevant for state-of-the-art multibeam systems employing partial frequency reuse [10] –different portions of the available spectrum are assigned to adjacent beams to reduce interference–, where each beam is processed separately without exploiting the residual interference.

A. Summary of contributions

The following is an outline of the contributions of the paper.

- We explicitly derive the probability density function (PDF) of the rain attenuation in *natural units* (11), d_i, which is the exponentiation of a log-normal random variable (log-lognormal); then, after deriving an approximation of the Gaussian error function (50), we obtain an analytical, closed-form expression for any moment of the attenuation, $\mathbb{E}\left[d_i^k\right], k > 0$ (14).
- For the multibeam antenna pattern, an analytical model based on Wyner's 2D cellular arrangement is obtained

(3). Its isolation parameter is determined by emulating a typical antenna's radiation pattern through the method of the Bessel functions (8).

- The ergodic capacity of the link is briefly studied, obtaining analytical expressions at low (23) and high (24) SNR. The obtained expressions suggest a mild influence of rain attenuation on the ergodic capacity.
- Regarding the outage capacity of the link, we derive approximations for the high and low SNR regimes (31), (36), which tightly fit simulation data[1].
- The outage capacity results can be particularized to the scalar, single-user channel. In such case, a general expression for any SNR can be found (42), as well as insightful particular versions for the low (44) and high (45) SNR regimes.
- Table I summarizes the results obtained regarding outage capacity (L and H stand for low and high SNR, respectively).

B. Structure and notation

The structure of the paper is the following: Section II describes the system model and details the proposed antenna pattern; Section III contains the derivations of the ergodic and outage capacity of the multibeam return link, along with the particularization for a single beam; Section IV reports simulation results to illustrate the accuracy of the derived expressions; finally, Section V summarizes the main results.

Notation: bold uppercase face $\mathbf{A}$ denotes matrices, bold lowercase $\mathbf{a}$ denotes (column) vectors, and $\mathbf{A}^H$ is the hermitean of $\mathbf{A}$; $\mathrm{diag}(\mathbf{A})$ is a column vector formed by the elements in the diagonal of matrix $\mathbf{A}$, while $\mathrm{diag}(\mathbf{a})$ is a diagonal matrix with elements given by $\mathbf{a}$. $\log(x)$ stands for the neperian logarithm of x; base-b logarithms are denoted as $\log_b(x)$. $\mathbb{E}[X]$ is the expectation operator over a random variable X.

II. SYSTEM MODEL

This paper focuses on a multi-user uplink, where multiple single-antenna terminals communicate towards a satellite equipped with a multi-feed reflector. We propose a beam pattern model and include the possibility of correlation among the rain attenuations experienced by different users –both dependent on the system geometry and inter-user distance.

Let us consider a multi-user channel with K single-antenna terminals transmitting towards a single satellite equipped with the same number of antennas (Figure 1), so that the signal model reads as

$$\mathbf{y} = \sqrt{\gamma}\mathbf{H}\mathbf{s} + \mathbf{n}, \tag{1}$$

where $\mathbf{s} \in \mathcal{C}^{K \times 1}$ is the transmitted signal vector, such that $\mathbb{E}[\mathbf{s}\mathbf{s}^H] = \mathbf{I}$, $\mathbf{y} \in \mathcal{C}^{K \times 1}$ is the received signal vector, $\mathbf{n} \sim \mathcal{CN}(\mathbf{0}, \mathbf{I})$ is the complex noise vector and γ is the transmit power over receiver noise (SNR). Matrix $\mathbf{H} \in \mathcal{C}^{K \times K}$ represents the complex-valued channel and can be expressed as [19]

$$\mathbf{H} = \mathbf{B}\mathbf{D} \tag{2}$$

---

[1]Although the resulting expression has been particularized for the proposed antenna model, any other model could be used instead.
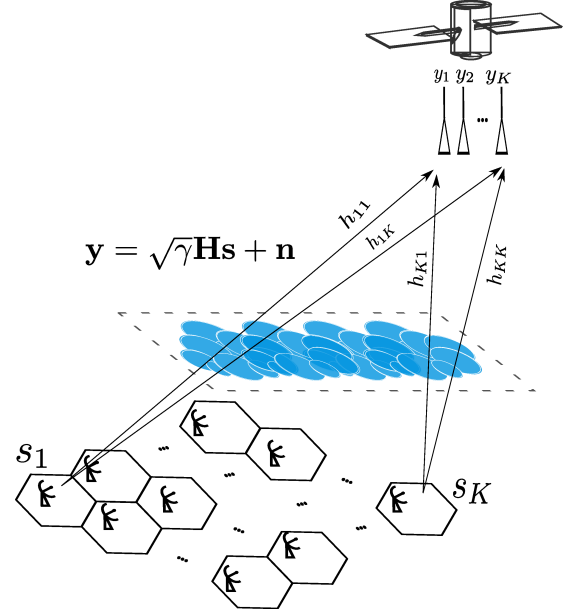

Figure 1. Diagram of the satellite return link under study.

where $\mathbf{B} \in \mathcal{C}^{K \times K}$ is a full column-rank matrix containing the antenna radiation pattern, and $\mathbf{D} = \mathrm{diag}(\boldsymbol{\delta})$, $\mathbf{D} \in \mathcal{C}^{K \times K}$, is a diagonal matrix of random entries modeling the rain attenuation coefficients.

We shall remark that γ refers to a normalized power over noise constant, which does not take interference into account. Inter-user interference is present in matrix $\mathbf{B}$, and in the attenuation experienced by the different users through $\mathbf{D}$. This will be made clearer through the following paragraphs.

A. Antenna pattern

In many practical instances, the antenna pattern is obtained by means of specific software, which models real antennas and components and yields the numerical entries of matrix $\mathbf{B}$.

For analytical purposes, we will rather use a mathematical model that allows to write $\mathbf{B}$ as a function of key system parameters, like the inter-user distance or the beam radius. In short, we will resort to a well-known information theoretic cellular model, namely Wyner's 2D model [20], to describe the geometry of the system. Using this model, $\mathbf{B}$ will be a function of a, the *isolation parameter* between adjacent beams; to model this parameter, we will use the well-accepted Bessel function antenna model for tapered-aperture antennas [21, p. 184], [22].

1) Wyner model: Similarly to [19], we describe the geometry of the beam coverage using Wyner's 2D arrangement of cells. This arrangement is achieved by considering L lines, each of M cells (so that $K = LM$), placed one on top of another, where *each cell is affected by a single tier of interfering cells*; this renders the channel matrix to a Toeplitz-Block-Toeplitz (TBT) matrix of the form

		Single user		Multiple users
C_ϵ	L	$\log_2\left(1 + \gamma \cdot e^{-e^{\sigma Q^{-1}(\epsilon)+\beta}}\right)$	$C_{\mathrm{awgn}} \cdot e^{-e^{\sigma Q^{-1}(\epsilon)+\beta}}$	$\sqrt{V_{\mathrm{L}}} \cdot Q^{-1}(1-\epsilon) + C_{\mathrm{low}}$
	H		$C_{\mathrm{awgn}} - e^{\sigma Q^{-1}(\epsilon)+\beta} \cdot \log_2 e$	$C_{\mathrm{awgn}} - e^{Q^{-1}(\epsilon)\Omega + M_{\mathrm{H}}}$

μ, σ are the location and scale parameters of the rain distribution, γ the SNR, $\beta = \mu - 2.1617$, C_{awgn} the capacity of an unfaded channel, C_{low} is the ergodic capacity at low SNR, $\Omega, M_{\mathrm{H}}, V_{\mathrm{L}}$ are parameters of the obtained approximations, defined in (32), (33), (37), respectively.

$$\mathbf{B} = \mathbf{T}_{2D} = \begin{pmatrix} \mathbf{T}_{1D} & \mathbf{S} & 0 & \ldots & 0 \\ \mathbf{S}^H & \mathbf{T}_{1D} & \mathbf{S} & \ddots & \vdots \\ 0 & \mathbf{S}^H & \mathbf{T}_{1D} & \ddots & 0 \\ \vdots & \ddots & \ddots & \ddots & \mathbf{S} \\ 0 & \ldots & 0 & \mathbf{S}^H & \mathbf{T}_{1D} \end{pmatrix}, \quad (3)$$

where

$$\mathbf{S}^T = \begin{pmatrix} a & a & 0 & \ldots & 0 \\ 0 & a & a & \ddots & \vdots \\ & 0 & a & \ddots & 0 \\ \vdots & & \ddots & \ddots & a \\ 0 & \ldots & & 0 & a \end{pmatrix}, \quad (4)$$

and

$$\mathbf{T}_{1D} = \begin{pmatrix} 1 & a & 0 & \ldots & 0 \\ a & 1 & a & \ddots & \vdots \\ 0 & a & 1 & \ddots & 0 \\ \vdots & \ddots & \ddots & \ddots & a \\ 0 & \ldots & 0 & a & 1 \end{pmatrix} \quad (5)$$

where a is the so-called isolation parameter, and with $\mathbf{S} \in \mathbb{R}^{M \times M}$, $\mathbf{T}_{1D} \in \mathbb{R}^{M \times M}$ and $\mathbf{T}_{2D} \in \mathbb{R}^{LM \times LM}$.

Remark: Assuming each cell to be affected by a single tier of interfering cells is, in fact, more realistic in multibeam satellite systems than in terrestrial scenarios, since in the former interbeam interference is solely controlled by the antenna design, and not by the terrain characteristics.

A drawback of the model above is that there is no closed-form expression for the eigenvalues of $\mathbf{T}_{2D}$. However, in the limit when $L, M \to \infty$, the eigenvalues of the TBT matrix of (3) are given by [23]:

$$\lambda_{(l-1)M+m}(\mathbf{T}_{2D}) = 1 + $$
$$2a\left(\cos\left(\frac{2\pi l}{L}\right) + \cos\left(\frac{2\pi m}{M}\right)\right. \quad (6)$$
$$\left. + \cos\left(\frac{2\pi l}{L} + \frac{2\pi m}{M}\right)\right),$$
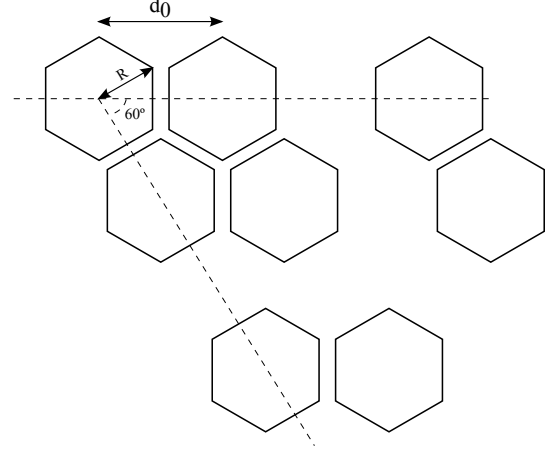
and we can exploit this for large systems.

Figure 2. Example of fixed beam patterns with changing distance between users; d_0, a parameter that we will vary through the analysis, is the distance between the centers of adjacent beamspots.

2) Modeling a: Using the Bessel function model for a typical tapered-aperture antenna [21, p. 184], [22], the channel gain from the i-th beam towards the j-th user is given by

$$g_{ij}(\theta_{ij}) = G_{\max}\left(\frac{J_1(u_{ij})}{2u_{ij}} + 36\frac{J_3(u_{ij})}{u_{ij}^3}\right)^2 \quad (7)$$

as a function of the off-axis angle with respect to the beam's boresight, $\theta_{ij} = \arctan(d_{ij}/D)$, where D is the distance from the user to the satellite and d_{ij} is the distance between the i-th beam boresight and the j-th user (or, equivalently, the distance between the center of the i-th and j-th cells). In the equation above, $u_{ij} = 2.07123 \sin\theta_{ij} / \sin\theta_{3\mathrm{dB}}$, J_1 and J_3 are the Bessel functions of the first kind, of order one and three respectively, $G_{\max}$ is the maximum axis gain of each antenna, and $\theta_{3\mathrm{dB}}$ is the angle associated to the beam's $3\,\mathrm{dB}$ radius, $\theta_{3\mathrm{dB}} = \arctan(R/D)$, with R the beam's radius.

For the sake of the analysis, the following approximations can be made: we will assume that the Earth curvature is negligible, that the slant ranges among all users are identical and equal to the GEO satellite elevation distance, $D = 36,000\,\mathrm{Km}$, that all users are placed in the centers of the beams, and that each beam's radiation pattern is fixed: as the distance between users changes, so will the centers of the fixed radius beams (see Figure 2).

Under the aforementioned assumptions, and since the distance among users is much smaller than the satellite altitude, the relative distance d is translated into an angle simply via
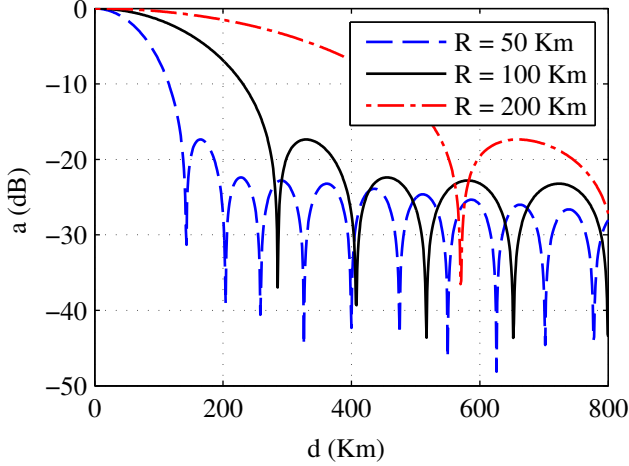
Figure 3. Evolution of the antenna pattern with respect to the beam center for different beam radius. Different link budgets have been used to enforce the same maximum gain.

$\theta \approx \frac{d}{D}$, and we finally have (see Figure 3):

$$a = \sqrt{\frac{g(\theta)}{G_{\max}}} = \frac{J_1(u)}{2u} + 36\frac{J_3(u)}{u^3}, \qquad (8)$$

$$u \approx 2.07123 \cdot d/R. \qquad (9)$$

B. Rain attenuation

The elements δ_i of the diagonal rain attenuation matrix $\mathbf{D} = \mathrm{diag}(\boldsymbol{\delta})$ follow [24]

$$-20\log_{10}(\delta_i) \sim \mathcal{LN}(\mu_i, \sigma_i) \qquad (10)$$

where μ_i and σ_i are the log-normal location and scale parameters, respectively, expressed in dB. Under this assumption, both δ and δ^2 follow a double log-normal distribution, as defined below.

Definition 1. *Let Y be a log-normally distributed random variable with location parameter μ and scale parameter σ, $Y \sim \mathcal{LN}(\mu, \sigma)$. Then, a random variable $X = A^{-\alpha Y}$ is said to be a double log-normal or log-lognormal random variable with scale parameter σ and location parameter $\beta \doteq \mu + \log\log A + \log\alpha$, $X \sim \mathcal{L}^2\mathcal{N}(\beta, \sigma)$.*

Lemma 1 (PDF and CDF of a $\mathcal{L}^2\mathcal{N}$ random variable)**.** *The PDF of a double log-normal random variable is given by [25]*

$$f_X(x) = -\frac{1}{\sqrt{2\pi}\sigma x \log x} \cdot e^{-\frac{1}{2\sigma^2}(\log(-\log x)-\beta)^2} \qquad (11)$$

with $0 < x < 1$, while the CDF is given by

$$F_X(x) = Q\left(\frac{\log(-\log x) - \beta}{\sigma}\right) \qquad (12)$$

with $Q(x)$ representing the widely used Gaussian Q-function.

Proof: Consider the function $g(x) = A^{-\alpha x}$, and that we wish to obtain the PDF of the transformation $g(Y)$; the result

follows immediately after considering that the inverse transformation is given by $-1/(\alpha \log A)\log x$, while its derivative equals $1/(\alpha x \log A)$. ∎

From the definitions above, it is clear that δ corresponds to $\alpha = 1/20$ and δ^2 to $\alpha = 1/10$.

The moments of δ^2 are not available in closed-form, since this would require solving

$$\int_0^1 \frac{x^{k-1}}{\log x} \cdot e^{-\frac{1}{2\sigma^2}(\log(-\log x)-\beta)^2} \, \mathrm{d}x. \qquad (13)$$

However, a closed-form expression can be obtained after resorting to a sigmoid approximation of the error function, as shown below.

Lemma 2. *Assume a tight approximation of the error function in the interval $[0, u/\sqrt{2})$, $u > 0$, given by $\mathrm{erf}(x) \approx \sum_{i=1}^{N_c} a_i e^{-b_i x}$ and the sets of coefficients $\{a_i\}_{i=1}^{N_c}$, $\{b_i\}_{i=1}^{N_c}$. Then, the k-th moment of the random variable $X \sim \mathcal{L}^2\mathcal{N}(\beta, \sigma)$, $M_X(k)$, can be approximated as shown in (14), where $\varsigma_j \doteq \frac{b_j}{\sqrt{2}\sigma}$ and $\Gamma(a, x)$ is the upper incomplete Gamma function $\Gamma(c, x) = \int_x^\infty t^{c-1}e^{-t}\mathrm{d}t$ [26, Eq. 6.5.3].*

Proof: see Appendix A. ∎

C. Rain spatial correlation

Once characterized the marginal statistics of the rain coefficients d_i, the main interest is to evaluate their correlation and the corresponding impact on the return link capacity. Taking into account correlation, $\boldsymbol{\delta}$ verifies

$$-20\log_{10}(\log\boldsymbol{\delta}) \sim \mathcal{N}(\boldsymbol{\mu}, \mathrm{diag}(\boldsymbol{\sigma})\mathbf{R}\,\mathrm{diag}(\boldsymbol{\sigma})) \qquad (15)$$

where $\boldsymbol{\mu}$ and $\boldsymbol{\sigma}$ are the location and scale parameter vectors, respectively, and $\mathbf{R} = \{r'_{ij}\}$ is the matrix of correlation coefficients among the so-called reduced Gaussian variables $u_i = (-20\log_{10}(\log\delta_i) - \mu_i)/\sigma_i$.

There are many different models for r', as summarized in [27]. Here we will use the two-exponential model

$$r'_{ij} = p_b(d_{ij}) \doteq 0.94e^{-\frac{d_{ij}}{30}} + 0.06e^{-\left(\frac{d_{ij}}{500}\right)^2}, \qquad (16)$$

which was adopted by ITU in ITU-R P. 618-10 [28], although introducing any other model would be straightforward.

In what refers to the associated log-normal random variables, their correlation is given by [18]

$$\rho_{ij} = \frac{e^{\sigma_i\sigma_j p_b(d_{ij})} - 1}{\sqrt{e^{\sigma_i} - 1}\sqrt{e^{\sigma_j} - 1}}. \qquad (17)$$

We will further impose $\mu_i \approx \mu, \sigma_i \approx \sigma \; \forall i$, so that the above equation simplifies to[2]

$$\rho_{ij} = \frac{e^{\sigma^2 p_b(d_{ij})} - 1}{e^{\sigma^2} - 1}. \qquad (18)$$

Differently from the antenna pattern, for the rain correlation we will consider the influence of all the cells, and not only

---

[2]In reality, the values of μ and σ measured in relatively close areas experience some small differences. However, since we will focus on the case where some degree of correlation exists among the rain attenuation coefficients, it is sensible to assume that the marginal statistics will be very similar.

$$2M_X(k) \approx e^{-k \cdot e^{\beta - u\sigma}} - e^{-k \cdot e^{\beta + u\sigma}}$$
$$+ \sum_{j=1}^{L} a_j \left(ke^\beta\right)^{\varsigma_j} \left(\Gamma\left(1 - \varsigma_j, ke^\beta\right) - \Gamma\left(1 - \varsigma_j, ke^{\beta + u\sigma}\right) + \left(ke^\beta\right)^{-2\varsigma_j} \Gamma\left(1 + \varsigma_j, ke^\beta\right) - \left(ke^\beta\right)^{-2\varsigma_j} \Gamma\left(1 + \varsigma_j, ke^{\beta - u\sigma}\right) \right) \quad (14)$$

the adjacent ones. The distance between the centers of any i-th and j-th cells is given by

$$d_{ij} = 3d_0\sqrt{(x_j - x_i)^2 + (y_j - y_i)^2 + (x_j - x_i)(y_j - y_i)} \quad (19)$$

with

$$x_i = \left\lfloor \frac{i}{M} \right\rfloor + 1, \quad y_i = i - \left\lfloor \frac{i}{M} \right\rfloor M \quad (20)$$

and d_0 the distance between the centers of adjacent hexagons, as shown in Figure 2.

Let $\mathbf{P}$ be the matrix of correlation coefficients, $\mathbf{P}_{ij} = \rho_{ij}$. For notational convenience, we will write $\mathbf{P}$ as

$$\mathbf{P} = \frac{1}{e^{\sigma^2} - 1}(\mathbf{A} - 1) \quad (21)$$

with $\mathbf{A}_{ij} \doteq e^{\sigma^2 p_b(d_{ij})}$.

III. PERFORMANCE UNDER CORRELATED RAIN ATTENUATION

We will start by briefly addressing the ergodic capacity of a multibeam satellite system; as we will see, rain correlation has no effect on this metric. We will then study the outage capacity of the channel, and assess the impact of the system's geometry and of the rain characteristics.

A. Ergodic capacity

For the channel under discussion, ergodic capacity is obtained by the well-known *logdet* formula $C_{\text{erg}} = \mathbb{E}_{\mathbf{D}}\left[\log_2 \det\left(\mathbf{I} + \gamma\mathbf{D}^2\mathbf{B}^H\mathbf{B}\right)\right]$. The expectation of the logarithm of the determinant is difficult to obtain, since it would require an analytical characterization of the (stochastic) eigenvalues of the product $\mathbf{D}^2\mathbf{B}^H\mathbf{B}$; instead, we will focus on the high and low SNR regimes.

Theorem 1. *The achievable sum rate can be approximated at low SNR by:*

$$C_{\text{low}} = \gamma \cdot M_\delta(2)\, \text{trace}\left(\mathbf{B}^H\mathbf{B}\right)\log_2 e \quad (22)$$

which, for the antenna model proposed in Section II-A, particularizes to

$$\begin{aligned} C_{\text{low}} = &\gamma \cdot M_\delta(2)\log_2 e \\ &\times \left(2a^2(3LM - 2L - 2M + 1) + LM\right) \end{aligned} \quad (23)$$

with a^2 from (8) ; $M_\delta(2) = \mathbb{E}\left[\delta^2\right]$ can be obtained from (14). On the other hand, at high SNR it would read as

$$C_{\text{high}} = C_{\text{awgn}} - \frac{\log_2 10}{10}K \cdot e^{\mu + \sigma^2/2} \quad (24)$$

with C_{awgn} obtained either numerically from $\mathbf{B}$, or by (25) for large systems.

Proof: At low SNR, using $\log(1 + x) \approx x$, the achievable sum rate is

$$\begin{aligned} C_{\text{low}} &= \gamma\mathbb{E}\left[\text{trace}\left(\mathbf{D}^2\mathbf{B}^H\mathbf{B}\right)\right]\log_2 e \\ &= \gamma\mathbb{E}\left[\delta^2\right]\text{trace}\left(\mathbf{B}^H\mathbf{B}\right)\log_2 e \end{aligned} \quad (26)$$

where the last equality follows from assuming the same attenuation statistics in all the paths; the extension to different statistics is straightforward and can be found in [1].

In what refers to $\text{trace}\left(\mathbf{B}^H\mathbf{B}\right)$, its value can be computed in closed form and results into (see Appendix B for the proof)

$$\text{trace}\left(\mathbf{B}^H\mathbf{B}\right) = 2a^2(3LM - 2L - 2M + 1) + LM, \quad (27)$$

so that substituting the value of a^2 completes the proof. ∎

Remark: The high SNR approximation holds whenever $\mathbf{I} \ll \gamma\mathbf{D}^2\mathbf{B}^H\mathbf{B}$, that is, when the system is not noise limited. For future satellite systems using strong frequency reuse, the system becomes strongly interference limited, and as a consequence high SNR analysis tend to be more relevant.

We have just shown how ergodic capacity can be expressed in a rain faded channel: at high SNR, it exhibits a constant loss with respect to the unfaded capacity, while at low SNR it amounts to a scaling of such unfaded capacity which depends on the rain statistics and antenna characteristics; similar problems had been tackled, among others, in [29], in that case by upper bounding capacity. However, we should question the importance of this metric for the channel under discussion.

It is well-known that, as the codeword length approaches infinity, the maximum rate at which reliable communication is possible approaches $\mathbb{E}\left[\log_2 \det\left(\mathbf{I} + \gamma\mathbf{D}^2\mathbf{B}^H\mathbf{B}\right)\right]$ [30]. But this is not the case of rain-faded satellite links, because codewords usually span only a few realizations of the channel[3]; this is called *slow fading*. In this case, ergodic capacity represents only the average rate at which we can transmit if we have perfect CSI at the transmitter (and without assuming any power allocation over time).

Also, note that the multiuser case has an additional motivation for further analysis: from the derived expressions (23) and (24), the correlation among the users rain attenuation has no effect on the ergodic capacity. As a consequence, this metric does not allow us to assess the induced system degradation. For these reasons, we will focus our analysis on the outage capacity of the link.

Before going further into the outage analysis, Figure 4 plots the evolution of the average and instantaneous capacity for different levels of correlation; the mean is always the same, but the dispersion of the dots is much higher for the case with

---

[3]This could be fixed by introducing an arbitrarily large interleaver, but this would come at the price of an arbitrarily large delay, unaffordable in our scenario.

$$C_{\text{awgn}} \approx \prod_{l=1}^{L} \prod_{m=1}^{M} \left(1 + \left(1 + 2a \left(\cos\left(\frac{2\pi l}{L}\right) + \cos\left(\frac{2\pi m}{M}\right) + \cos\left(2\pi\left(\frac{l}{L} + \frac{m}{M}\right)\right) \right) \right)^2 \right) \qquad (25)$$
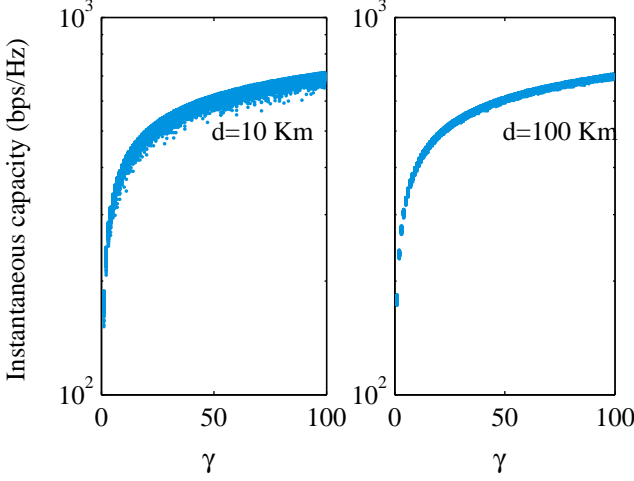

Figure 4. Realizations of $\log_2 \det\left(\mathbf{I} + \gamma \mathbf{D}^2 \mathbf{B}^H \mathbf{B}\right)$ for two levels of correlation of the entries in $\mathbf{D}$, and fixing $\mathbf{B}$.

higher correlation (left). In short, the average rate will not be much lower but the availability of the link will suffer the most. We will now analyze all these effects in more detail.

B. Outage capacity

As stated, correlation among the diagonal elements in $\mathbf{D}$ has no effect on ergodic capacity because it does not affect the expectation

$$C_{\text{erg}} = \sum_i \mathbb{E}_{\mathbf{D}} \left[\log_2(1 + \gamma \lambda_i \{\mathbf{D}^2 \mathbf{B}^H \mathbf{B}\}) \right] \qquad (28)$$

where λ_i denotes the i-th largest eigenvalue of a matrix. However, other metrics are greatly affected by the fluctuations of the random variable $\mathcal{I} = \sum_i \log_2(1 + \gamma \lambda_i \{\mathbf{D}^2 \mathbf{B}^H \mathbf{B}\})$.

In a slow fading channel, for a given rate R, the probability that the instantaneous capacity is lower than R is given by the outage probability

$$p_{\text{out}}(R) \doteq \mathrm{P}\left[\mathcal{I} < R\right] \qquad (29)$$

where $\mathcal{I}$ is the instantaneous capacity.

Also of highly practical significance is the ϵ-outage capacity, that is, the largest transmission rate at which the outage probability is less than ϵ [30], [31]. In other words: the maximum rate the channel will allow with probability $1 - \epsilon$.

In our case, from (29), we have that C_ϵ is the maximum value satisfying

$$\mathrm{P}\left[\log_2 \det\left(\mathbf{I} + \gamma \mathbf{D}^2 \mathbf{B}^H \mathbf{B}\right) < C_\epsilon\right] = \epsilon. \qquad (30)$$

Let us analyze this expression for the high and low SNR regimes.

Theorem 2. *At high SNR, the outage capacity can be approximated by*

$$C_\epsilon^{\text{H}} = C_{\text{awgn}}^{\text{H}} - e^{Q^{-1}(\epsilon)\Omega + M_{\text{H}}} \qquad (31)$$

with

$$\Omega^2 = \log\left(e^{\sigma^2} + \frac{2}{K}S\right) - \log K, \qquad (32)$$

$$M_{\text{H}} = \mu + \frac{\sigma^2}{2} - \frac{1}{2}\log\left(e^{\sigma^2} + \frac{2}{K}S\right) \\ + \frac{3}{2}\log K + \log\left(\frac{\log_2 10}{10}\right), \qquad (33)$$

$$S \doteq \sum_{\substack{i,j \\ i<j}} \mathbf{A}_{ij}. \qquad (34)$$

Proof: See Appendix C. ∎

What (31) tells us is that, at high SNR, rain induces a constant loss also in terms of outage capacity. This loss depends on S in (34), which is a function of the inter-user distance and of the rain geometry model used, but it does not depend on the SNR γ. In particular, the loss grows with S, which is a sum of elements which increase exponentially with the correlation value. As a consequence, decreasing the distance (increasing correlation) makes the loss grow sharply, as we will see in Section IV. However, decreasing the distance would also affect $\mathbf{B}$. The overall effect thus depends also on the particular beam pattern under use. Note that these same expressions would hold for any other model, as long as we are able to compute the summation that leads to S.

Following the model we proposed, C_{awgn} also depends on $\mathbf{B}$. Since in (31) the contributions of the antenna pattern and of the rain are decoupled, it would be easy to extend the analysis to any other antenna model. We will exploit this to illustrate the influence of rain alone in Section IV.

A final remark concerns the case with only one user: noting that $K = 1$ and $S = 0$, we can easily particularize (31) and obtain

$$C_\epsilon^{\text{H}} = C_{\text{awgn}}^{\text{H}} - e^{Q^{-1}(\epsilon)\sigma + \mu + \log\left(\frac{\log_2 10}{10}\right)} \qquad (35)$$

which, interestingly, is the expression of the outage capacity for a single-user channel impaired by rain attenuation at high SNR, as we will show in the next section.

Theorem 3. *At low SNR, and under moderate correlation, the outage capacity can be approximated by*

$$C_\epsilon^{\text{L}} \approx \sqrt{V_{\text{L}}} \cdot Q^{-1}(1 - \epsilon) + C_{\text{low}} \qquad (36)$$

where C_{low} is given by (22), and with

$$V_{\text{L}} = (\log_2 e)^2 \gamma^2 \\ \times \left(M_\delta(4) \sum_{i=1}^{K} ||\mathbf{b}_k||^4 + 2 \sum_{\substack{i,j \\ i<j}} \varphi_{i,j} \cdot ||\mathbf{b}_i||^2 ||\mathbf{b}_j||^2 \right) \qquad (37) \\ - C_{\text{low}}^2,$$

$$\varphi_{i,j} \triangleq \mathbb{E}\left[\delta_i \delta_j\right] = \int_{-\infty}^{\infty} \int_{-\infty}^{\infty} 10^{-\frac{1}{10}\left(e^{\sigma x + \mu} + e^{\sigma y + \mu}\right)} \tag{38}$$
$$\times f(x,y)\,\mathrm{d}x\mathrm{d}y,$$

and $f(x,y)$ the PDF of a bivariate Gaussian distribution,

$$f(x,y) = \frac{1}{2\pi\sqrt{1-(r'_{i,j})^2}} \cdot e^{-\frac{1}{2(1-(r'_{i,j})^2)}\left(x^2 + y^2 - 2r'_{i,j}xy\right)}. \tag{39}$$

Proof: See Appendix D. ■

The value $Q^{-1}(1-\epsilon)$ is negative for $\epsilon < 0.5$. Thus, increasing V_{L} decreases the outage capacity.

Remark: Differently from the high SNR case, here the effect of the distance cannot be easily separated in antenna effects and correlation effects. Note that decreasing the distance will increase the values $\varphi_{i,j} = \mathbb{E}\left[\delta_i \delta_j\right]$, and will thus tend to decrease the outage capacity; however, decreasing the distance at the same time increases the values of $||\mathbf{b}_i||$ and of C_{low}. Summarizing: Theorem 3 is valid for any antenna pattern, but the shape of $C_{\epsilon}^{\mathrm{L}}$ as a function of the distance will depend on its particular values.

Remark: As explained in the appendix, the result above relies on approximating $\mathrm{trace}\left(\mathbf{D}^2\mathbf{B}^H\mathbf{B}\right)$ by a Gaussian random variable, which proves to be accurate whenever the correlation among the elements in $\mathbf{D}$ is not very high. For this latter case, the trivial approximation $\mathbf{D} \approx \delta\mathbf{I}$, with δ a single log-lognormal random variable, should be used instead.

C. The single-user case

So far, we have tackled the multi-antenna, multiuser case, showing that the outage induced by rain is constant at high SNR, and that it is larger when the rain correlation is stronger. The obtained results are relevant for systems employing full frequency reuse and joint multiuser detection.

In this section, we will explore the simplified case with only one user and one receiving antenna. Apart from yielding very illustrative results, this scenario has great operational significance, as it corresponds to the multibeam scenarios in which partial frequency reuse is employed; in such cases, adjacent beams are assigned different frequencies and it is customary to operate the link without exploiting the residual interference.

At time instant k, the signal model would be

$$y_k = \sqrt{\gamma} \cdot h_k s_k + n_k \tag{40}$$

where y_k and s_k are the received and transmitted symbols, respectively, h_k is the channel coefficient, n_k is a complex standard normal noise sample, $n_k \sim \mathcal{CN}(0,1)$, and γ is a variable that denotes the SNR taking into account all the deterministic coefficients of the link budget, including the noise power, the path losses, and any other attenuation in the transmission chain.

Solving (29) for $p_{\mathrm{out}} = \epsilon$ yields

$$C_\epsilon = \log_2\left(1 + F^{-1}(\epsilon) \cdot \gamma\right) \tag{41}$$

where F denotes the *cumulative distribution function* of $|h|^2$, so that substituting (12) in (41) we obtain

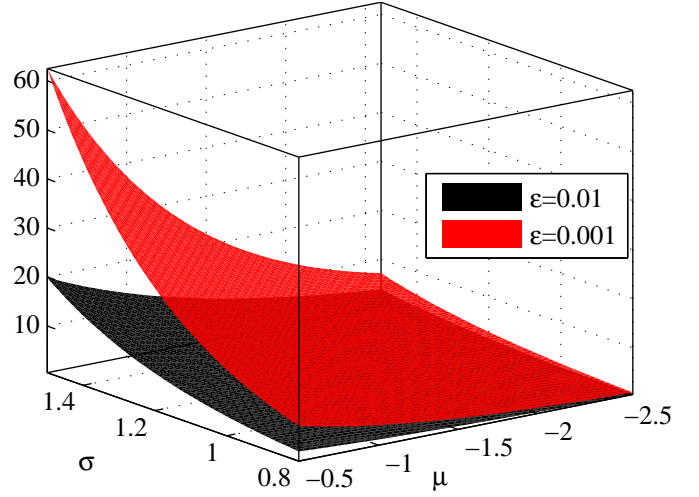$$C_\epsilon = \log_2\left(1 + \gamma \cdot e^{-e^{\sigma Q^{-1}(\epsilon) + \beta}}\right). \tag{42}$$

Figure 5. Evolution of Δ_P as a function of σ and μ for different values of ϵ.

An immediate conclusion from (41) is that, to obtain the same rate as in an AWGN channel –but with an outage probability of ϵ instead – we will need an extra power of

$$\Delta_P \doteq -10\log_{10} F^{-1}(\epsilon)$$
$$= e^{\sigma Q^{-1}(\epsilon) + \beta} \cdot 10\log_{10} e \text{ dB.} \tag{43}$$

We can see that an increase in the location parameter μ, present in β, exponentially increases the power loss term. The same behavior holds for the scale parameter σ, but this is *amplified* by the value of $Q^{-1}(\epsilon)$, which grows larger as ϵ decreases; this can be seen on Figure 5.

Even though the extra power margin needed is the same regardless of the power regime, the effect of fading on the outage capacity does change with the SNR, as we will see in the following.

Theorem 4. *The outage capacity at low SNR can be approximated by*

$$C_\epsilon^{\mathrm{L}} \approx C_{\mathrm{awgn}} \cdot e^{-e^{\sigma Q^{-1}(\epsilon) + \beta}}, \tag{44}$$

while at high SNR it reads as

$$C_\epsilon^{\mathrm{H}} \approx C_{\mathrm{awgn}} - e^{\sigma Q^{-1}(\epsilon) + \beta} \cdot \log_2 e. \tag{45}$$

Proof: Both identities can be proven by applying $\log_2(1+x) \approx x/\log 2$ when $0 < x << 1$ (low SNR) and $\log_2(1+x) \approx \log_2(x)$ (high SNR). ■

From the expressions above, it is easy to check that (45) is the same as (35) by substituting the expression of β; note that this equality happens even though in the multiuser case we had used an additional approximation, assuming that a sum of log-normally distributed random variables can be fit by a single log-normal random variable. Also, (44) tells us that the rain effect is quite different at low SNR: it scales capacity by a double exponential of $\sigma Q^{-1}(\epsilon) + \beta$.

IV. NUMERICAL RESULTS

In this section, we report some numerical results illustrating the behavior of a correlated rain-faded satellite return link.
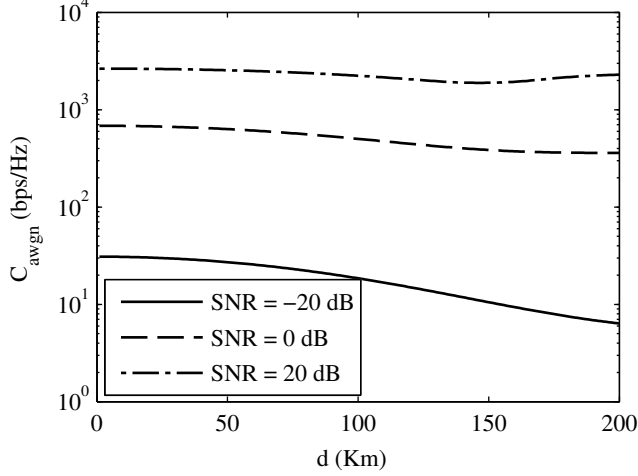
Figure 6. Capacity as a function of distance for the unfaded channel.

Figure 7. Outage capacity loss induced by rain as a function of d_0 for different values of ϵ.

Simulations have been carried out with $\mu = -1.013$, $\sigma = 1.076$, as obtained in [32] for the city of Aarhus; $R = 100$ Km; and $L = 10$, $M = 10$, so that $K = 100$.

Figure 6 shows the evolution of capacity as a function of the inter-user distance for different values of SNR (γ), in a setup with no rain attenuation; the aim of this figure is to depict only the influence of the deterministic antenna pattern, which resembles that shown in [19].

Now we wish to assess the outage capacity in the presence of spatially correlated rain attenuation; to start with, Figure 9 depicts the outage capacity as a function of distance for the high and low SNR cases. Judging from Figures 9 and 6, it would seem that outage capacity as a function of inter-user distance is affected mostly by changes in the antenna pattern, which lead to changes in C_{awgn}^H. This, however, does not have to be true for every antenna pattern: other patterns could exist for which C_{awgn}^H had a value comparable to $-e^{\Omega Q^{-1}(1-\epsilon)+M_{\mathrm{H}}}$.

Figure 10 shows the CDF of the instantaneous capacity at high and low SNR for different distance values. We can see the effect of inter-user distance in the way the curves are shifted, and also that the derived analytical approximations tightly fit the Monte Carlo simulation.

To illustrate the influence of rain alone at high SNR, Figure 7 shows the evolution of the term $-e^{Q^{-1}(\epsilon)\Omega+M_{\mathrm{H}}}$, which is the ϵ-capacity loss induced by rain attenuation, for different values of ϵ; we can see that, for example, with $\epsilon = 10^{-4}$ and $d = 100$ Km, the total loss equals about 42 bps/Hz, which roughly means 0.42 bps/Hz on average per user. Note that these losses are independent of the antenna pattern.

We can also get some insights on the behavior of outage capacity for the whole SNR range. Figure 8 shows its behavior for $\epsilon = 10^{-3}$, illustrating also the ranges of validity of the high and low SNR approximations. To this end, recall that the high SNR range is probably the most relevant, since it corresponds also to an interference limited case.

Before reporting the single user results, we will briefly analyze the effect of correlation over the rate of specific
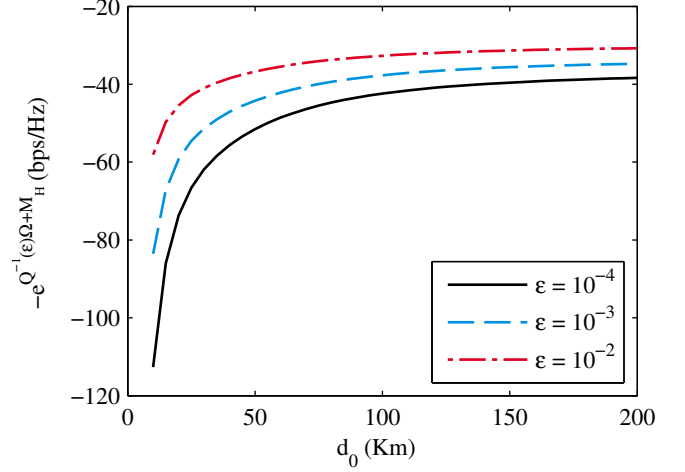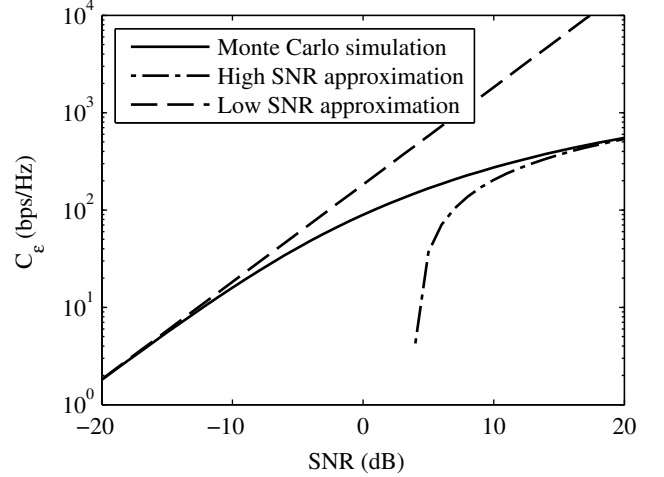

Figure 8. Outage capacity versus SNR, $\epsilon = 10^{-3}$.

users, rather than on the overall sum rate. For this purpose, Figure 11 shows the outage probability of the minimum and maximum rate –that is, of the rate of the user in the worst and best conditions, respectively– obtained after simulating the successive decoding of the users. For this simulation, we have selected in each iteration the user j with the largest value of $||\mathbf{h}_j||^2$, obtained its rate, and then removed the j-th column from the channel matrix. Correlation can be seen to have almost no effect on the minimum rate, but rather a significant impact on the maximum rate.

Finally, we present some results regarding the single-user scenario; we will rather depict $C_\epsilon/C_{\mathrm{awgn}}$. Figure 12 shows the derived approximations together with the original curve. We can see that, with the same power as in clear sky conditions, ensuring an availability of $99.999\,\%$ would imply reducing the rate down to a $10\,\%$ at low SNR, and even as low as $30\,\%$ for moderate SNR values like 10 dB.
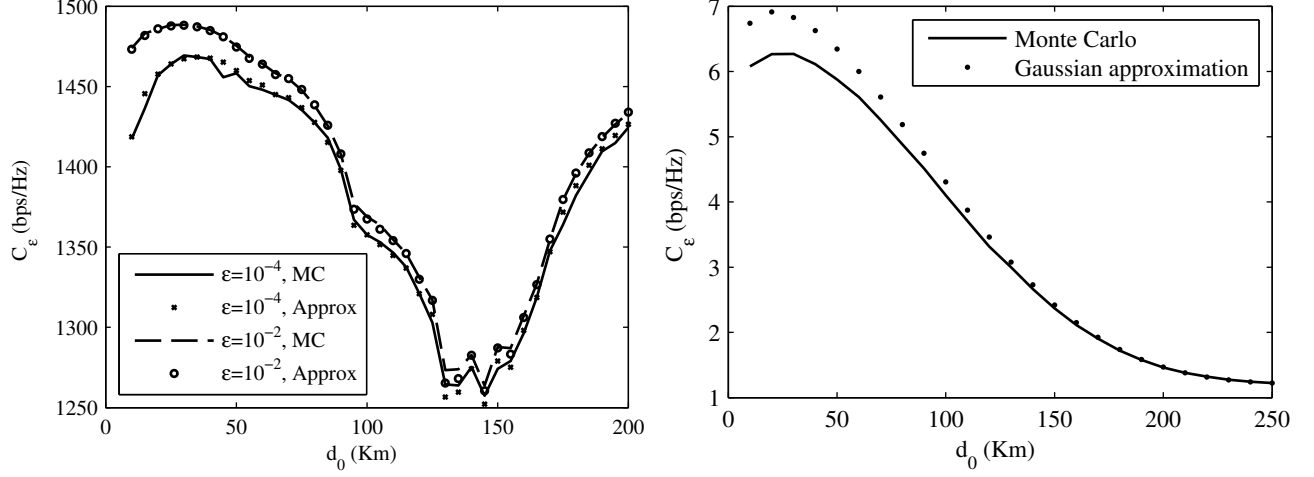
Figure 9. C_ϵ as a function of d_0 at high SNR (left, $45\,\mathrm{dB}$) and low SNR (right, $-20\,\mathrm{dB}$).
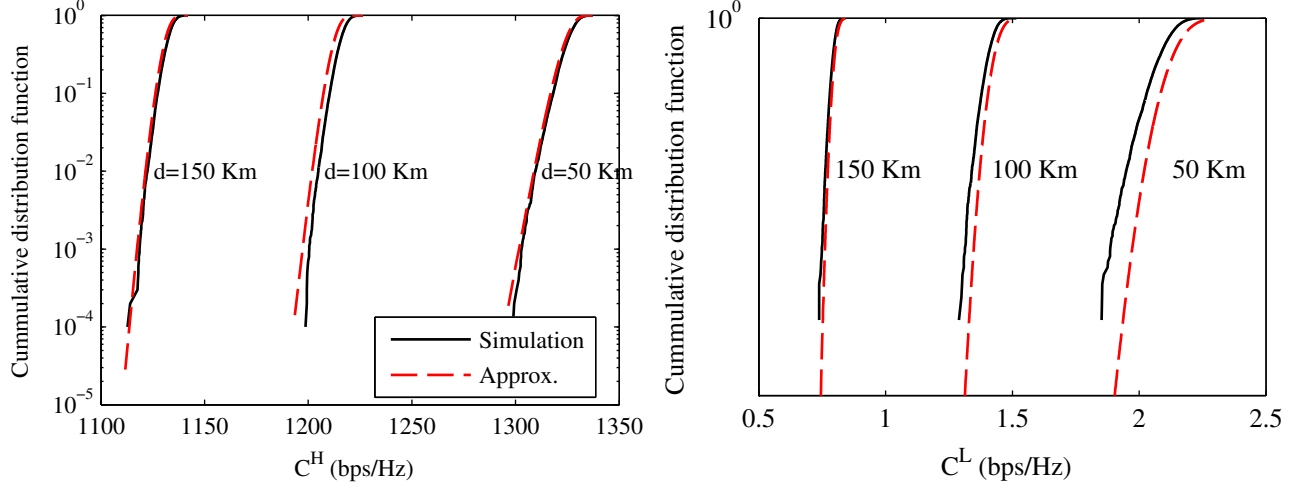
Figure 10. CDF of the instantaneous capacity at high (left, $40\,\mathrm{dB}$) and low (right, $-20\,\mathrm{dB}$) SNR for different values of d.
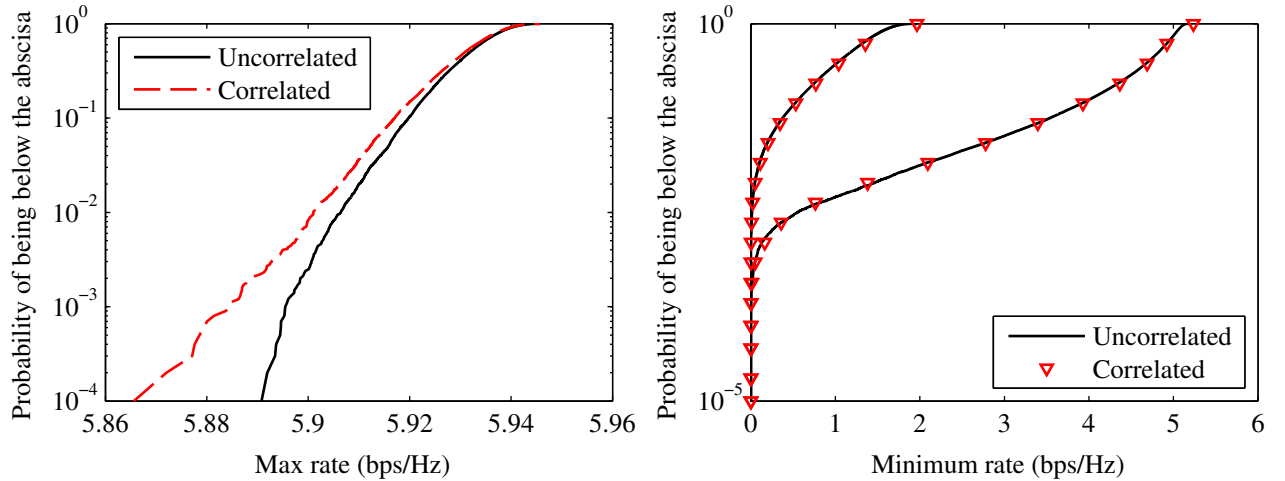

Figure 11. Outage probability of the maximum rate with $\mathrm{SNR} = 10\,\mathrm{dB}$ (left), and of the minimum rate on the right; for the latter, upper lines show $\mathrm{SNR} = 40\,\mathrm{dB}$, lower lines $\mathrm{SNR} = 10\,\mathrm{dB}$.
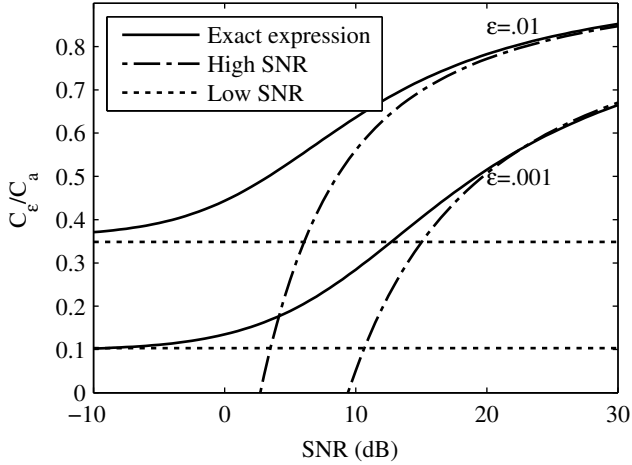
Figure 12. Accuracy of the high and low SNR approximations for $\epsilon = 0.01$ and $\epsilon = 0.001$. $\mu = -2.6$ dB and $\sigma = 1.3$ dB.

V. CONCLUSIONS

We have studied the effect of spatially correlated rain attenuation on a multibeam satellite return link from the point of view of outage capacity.

Results have shown that inter-user distance affects both the antenna pattern and the correlation among the beams. Focusing only on the latter, we have seen that correlation induces noticeable losses on the outage capacity of the system. For example, with $\epsilon = 10^{-4}$, an inter-user distance of $100\,\mathrm{Km}$ and a beam radius of $100\,\mathrm{Km}$, the total loss equals about $42\,\mathrm{bps/Hz}$, which roughly means $0.42\,\mathrm{bps/Hz}$ in average per user.

For the particular case of a single user, single antenna link, results have shown that ensuring an outage probability of 10^{-3} requires an extra power offset of about $15\,\mathrm{dB}$ for common rain profiles. In terms of outage capacity, this means reaching only $10\,\%$ of the unfaded capacity at low SNR and $65\,\%$ at high SNR if we do not increase the power margin.

VI. ACKNOWLEDGEMENTS

APPENDIX A
APPROXIMATION OF THE MOMENTS OF THE LOG-LOGNORMAL DISTRIBUTION

Here, we derive a semi-analytical formula for the moments of X, which needs of a tight approximation of the error function $\mathrm{erf}(x)$ in the positive interval; once the approximation is available, the expression of the moments follows in closed form.

Before starting, let us state an important property of the log-lognormal distribution: if $X \sim \mathcal{L}^2\mathcal{N}(\beta, \sigma)$, then for any $k > 0$ it holds that

$$X^k \sim \mathcal{L}^2\mathcal{N}(\beta + \log k, \sigma). \qquad (46)$$

This property will be very useful for the computation of the moments $\mathbb{E}\left[X^k\right]$.

To start with, let us reformulate the problem in a more convenient way.

Lemma 3. *Let $M_X(k)$ be the k-th moment of the random variable X. If X follows a log-lognormal distribution, then its computation can be rewritten as*

$$M_X(k) = \frac{1}{2} - \frac{1}{2}\int_0^\infty \mathrm{erf}\left(\frac{\beta + \log k - \log z}{\sqrt{2}\sigma}\right) e^{-z}\,\mathrm{d}z. \quad (47)$$

Proof: Recall that the expectation of a non-negative random variable can be written as [33, Eq. (5-53)]

$$\mathbb{E}[X] = \int_0^\infty \left(1 - F_X(x)\right)\,\mathrm{d}x. \qquad (48)$$

Now, noting that $Q(x) = 1/2 - 1/2 \cdot \mathrm{erf}\left(x/\sqrt{2}\right)$ and $\mathrm{erf}(-x) = -\mathrm{erf}(x)$, we arrive at

$$\begin{aligned}
\mathbb{E}[X] &= \int_0^1 \left(1 - Q\left(\frac{\log(-\log x) - \beta}{\sigma}\right)\right)\,\mathrm{d}x \\
&= \frac{1}{2} - \frac{1}{2}\int_0^1 \mathrm{erf}\left(\frac{\beta - \log(-\log x)}{\sqrt{2}\sigma}\right)\,\mathrm{d}x.
\end{aligned} \qquad (49)$$

The proof concludes by using (46) and applying the change of variables $\log x = -z$. ∎

Unfortunately, the integral in (47) still appears to be intractable. At this point, we will look for a good substitute for $\mathrm{erf}(x)$ in an interval of the form $[0, r)$ that allows to compute the integral in closed form and, at the same time, offers good accuracy; the idea of focusing in a reduced interval is precisely to improve the accuracy by dealing with the asymptote $\mathrm{erf}(x) = 1$ separately. Well-known accurate existing approximations of the Q function, or of the error functions, involve exponentials of quadratic argument or polynomials (see [34] and references therein). Inspired in part by [35], we developed an approximation given by a sum of N_c exponentials of x:

$$\mathrm{erf}(x) \approx \sum_{i=1}^{N_c} a_i e^{-b_i x} \quad 0 \le x < r \qquad (50)$$

for $N_c > 1$.

Recall that looking for an approximation in a reduced interval $[0, r)$ aims at improving the accuracy in the curvy parts of the function; the almost constant values of $\mathrm{erf}(x)$ when x grows large could be handled separately by setting r to a small value, as we will show. Table II shows the optimized coefficients, which were obtained by applying non-linear mean-squared optimization in Matlab$^{©}$, for different values of N_c and $r = 5/\sqrt{2}$.

Table II
COEFFICIENTS OF THE APPROXIMATION (50) OF $\mathrm{erf}(x)$ FROM 0 TO $5/\sqrt{2}$

N_c	Coefficients
2	$a_1 = -1.295$, $a_2 = 1.24$, $b_1 = 1.346$, $b_2 = 0.06363$
4	$a_1 = 0.0027151$, $a_2 = -1.026$, $a_3 = 2$, $a_4 = -1.02$ $b_1 = -1.20$, $b_2 = 0.9814$, $b_3 = 0.2306$, $b_4 = 0.9814$

Once an approximation of the error function of the form of (50) is available, the moments of X can be computed in closed form: Let us focus on the case $k = 1$, since any other case would follow by a simple change of variables. We start by splitting the definite integral into two parts, so that the argument of $\mathrm{erf}(x)$ is always positive, thus resulting into

$$
\begin{aligned}
2M_X(1) = 1 &- \int_0^{e^\beta} \mathrm{erf}\left(\frac{\beta - \log z}{\sqrt{2}\sigma}\right) e^{-z}\,\mathrm{d}z \\
&+ \int_{e^\beta}^\infty \mathrm{erf}\left(-\frac{\beta - \log z}{\sqrt{2}\sigma}\right) e^{-z}\,\mathrm{d}z \\
&= 1 - I_1 + I_2.
\end{aligned}
\tag{51}
$$

We further split each integral to separate the part in which $\mathrm{erf}(x) \approx 1$:

$$
\begin{aligned}
I_1 &\doteq \int_0^{e^\beta} \mathrm{erf}\left(\frac{\beta - \log z}{\sqrt{2}\sigma}\right) e^{-z}\,\mathrm{d}z \\
&= 1 - e^{-e^{\beta - u\sigma}} + \int_{e^{\beta - u\sigma}}^{e^\beta} \mathrm{erf}\left(\frac{\beta - \log z}{\sqrt{2}\sigma}\right) e^{-z}\,\mathrm{d}z
\end{aligned}
\tag{52}
$$

The same operation applied on the second integral yields

$$
\begin{aligned}
I_2 &\doteq \int_{e^\beta}^\infty \mathrm{erf}\left(-\frac{\beta - \log z}{\sqrt{2}\sigma}\right) e^{-z}\,\mathrm{d}z \\
&= -e^{-e^{\beta + u\sigma}} + \int_{e^\beta}^{e^{\beta + u\sigma}} \mathrm{erf}\left(-\frac{\beta - \log z}{\sqrt{2}\sigma}\right) e^{-z}\,\mathrm{d}z.
\end{aligned}
\tag{53}
$$

The two unsolved integrals can be worked out in the same way. Picking the first one, we can apply the exponential sum approximation (50) to obtain

$$
\begin{aligned}
&\int_{e^{\beta - u\sigma}}^{e^\beta} \mathrm{erf}\left(\frac{\beta - \log z}{\sqrt{2}\sigma}\right) e^{-z}\,\mathrm{d}z \\
&\approx \sum_{j=1}^{N_c} a_j \int_{e^{\beta - u\sigma}}^{e^\beta} e^{-b_j \frac{\beta - \log z}{\sqrt{2}\sigma} - z}\,\mathrm{d}z \\
&= \sum_{j=1}^{N_c} a_j e^{-\varsigma_j \beta} \int_{e^{\beta - u\sigma}}^{e^\beta} z^{\varsigma_j} e^{-z}\,\mathrm{d}z \\
&= \sum_{j=1}^{N_c} a_j e^{-\varsigma_j \beta} \left(-\Gamma\left(1 + \varsigma_j, e^\beta\right) + \Gamma\left(1 + \varsigma_j, e^{\beta - u\sigma}\right)\right)
\end{aligned}
\tag{54}
$$

where the last equality follows from the definition of the upper incomplete Gamma function.

Applying the same procedure to the integral in I_2 and substituting in (51) concludes the proof. $\quad\square$

APPENDIX B
COMPUTATION OF trace $\left(\mathbf{B}^H\mathbf{B}\right)$

It is straightforward to check that the block-diagonal of $\mathbf{B}^H\mathbf{B}$ is formed by $L - 2$ matrices $\mathbf{S}^H\mathbf{S} + \mathbf{T}^2 + \mathbf{S}\mathbf{S}^H$ and 2 matrices $\mathbf{S}^H\mathbf{S} + \mathbf{T}^2$, so that

$$
\mathrm{trace}\left(\mathbf{B}^H\mathbf{B}\right) = L\,\mathrm{trace}\left(\mathbf{T}^2\right) + 2(L-1)\,\mathrm{trace}\left(\mathbf{S}^H\mathbf{S}\right) \tag{55}
$$

since $\mathrm{trace}(\mathbf{S}^H\mathbf{S}) = \mathrm{trace}(\mathbf{S}\mathbf{S}^H)$. The traces involved represent the Fröbenius norm of matrices $\mathbf{T}$ and $\mathbf{S}$, respectively. In other words, they represent the sum of the power of their columns. From this premise, they can be readily found to be

$$
\mathrm{trace}\left(\mathbf{S}^H\mathbf{S}\right) = a^2 + (M-1)2a^2 = a^2(2M - 1) \tag{56}
$$

and

$$
\begin{aligned}
\mathrm{trace}\left(\mathbf{T}^2\right) &= 2(1 + a^2) + (M - 2)(1 + 2a^2) \\
&= 2a^2(M - 1) + M.
\end{aligned}
\tag{57}
$$

The proof finishes immediately by combining the results above, yielding

$$
\mathrm{trace}\left(\mathbf{B}^H\mathbf{B}\right) = 2a^2(3LM - 2L - 2M + 1) + LM. \tag{58}
$$
$\quad\square$

APPENDIX C
PROOF OF THEOREM 2

The usual approximation results into

$$
\begin{aligned}
C &\approx \log_2 \det\left(\gamma\mathbf{D}^2\mathbf{B}^H\mathbf{B}\right) \\
&= \log_2 \det\left(\gamma\mathbf{B}^H\mathbf{B}\right) - \left(-\log_2 \det\mathbf{D}^2\right) \\
&= C_{\mathrm{awgn}}^{\mathrm{H}} - \Delta_c
\end{aligned}
\tag{59}
$$

where we have defined $\Delta_c \doteq -\log_2 \det\mathbf{D}^2$, the loss in spectral efficiency induced by rain attenuation

$$
\begin{aligned}
\Delta_c &= -\sum_{i=1}^{K} \log_2 \delta_i^2 \\
&= \frac{\log_2 10}{10} \sum_{i=1}^{K} \xi_i \qquad \xi_i \sim \mathcal{LN}\left(\mu, \sigma\right).
\end{aligned}
\tag{60}
$$

From (59) we have that the outage probability for a certain *overall rate* R is given by

$$
p_{\mathrm{out}}(R) = \mathrm{P}\left[C_{\mathrm{awgn}}^{\mathrm{H}} - \Delta_c < C_\epsilon\right] \tag{61}
$$

so that, solving $p_{\mathrm{out}}(C_\epsilon^{\mathrm{H}}) = \epsilon$ we obtain

$$
C_\epsilon^{\mathrm{H}} = C_{\mathrm{awgn}} - F_{\Delta_c}^{-1}(1 - \epsilon) \tag{62}
$$

where F_{Δ_c} is the cumulative distribution function (CDF) of Δ_c.

Let us see how can we obtain F_{Δ_c}. The sum of (correlated or uncorrelated) log-normal random variables has been extensively studied in the literature; a summary of the most relevant alternatives can be found in [36]. Here, and for simplicity, we will make use of Fenton-Wilkinson's approximation, which states that a sum of log-normal variables can be approximated by another log-normal variable by matching the first and second order moments.

Let us derive the expressions of these two moments, expressing them as a function of the correlation coefficients. The first moment, $\mu_1 \doteq \mathbb{E}[\Delta_c]$ trivially reads as

$$\mu_1 = \frac{\log_2 10}{10} \sum_{i=1}^{K} \mathbb{E}[\xi_i] = \frac{\log_2 10}{10} \cdot K e^{\mu + \frac{1}{2}\sigma^2} \qquad (63)$$

where we have used the fact that, if $x \sim \mathcal{LN}(\mu, \sigma)$, then $\mathbb{E}[x] = e^{\mu + 1/2\sigma^2}$.

The second order moment is more involved; using the binomial expansion

$$\left(\sum_{i=1}^{N} x_j \right)^2 = \sum_{i=1}^{N} x_i^2 + 2 \sum_{\substack{i,j \\ i<j}}^{N} x_i x_j \qquad (64)$$

we arrive at

$$\begin{aligned}
\mu_2 &= \frac{(\log_2 10)^2}{100} \mathbb{E}\left[\sum_{i=1}^{K} \xi_i^2 + 2 \sum_{\substack{i,j \\ i<j}}^{K} \xi_i \xi_j \right] \\
&= \frac{(\log_2 10)^2}{100} \left(K\mathbb{E}[\xi^2] + 2\sum_{\substack{i,j \\ i<j}}^{K} \left(\mathrm{var}(\xi)\rho_{ij} + \mathbb{E}[\xi^2] \right) \right) \\
&= \frac{(\log_2 10)^2}{100} \left(K\mathbb{E}[\xi^2] + 2\,\mathrm{var}(\xi) \sum_{\substack{i,j \\ i<j}}^{K} \rho_{ij} + 2\frac{K(K-1)}{2}\mathbb{E}[\xi]^2 \right).
\end{aligned} \qquad (65)$$

were we have used the fact that $\sum_{\substack{i,j \\ i<j}}^{K} 1 = K(K-1)/2$. We further use the following set of identities: $\mathbb{E}[\xi^2] = e^{2\mu+2\sigma^2}$, $\mathbb{E}[\xi]^2 = e^{2\mu+\sigma^2}$, $\mathrm{var}(\xi) = \left(e^{\sigma^2} - 1 \right) e^{2\mu+\sigma^2}$; plugging these expressions into (65), we get

$$\mu_2 = \frac{(\log_2 10)^2}{100} K e^{2\mu+\sigma^2} \left(e^{\sigma^2} + K - 1 + 2\frac{e^{\sigma^2}-1}{K}\sum_{\substack{i,j \\ i<j}}^{K} \rho_{ij} \right) \qquad (66)$$

Note that, as the correlation among the fading variables increases, the value of μ_2 also increases, thus resulting into an increase in variance.

Computing the pending summation in (66), we obtain

$$\begin{aligned}
\sum_{\substack{i,j \\ i<j}} \rho_{ij} &= \sum_{\substack{i,j \\ i<j}} \mathbf{P}_{ij} \\
&= \frac{1}{e^{\sigma^2}-1} \sum_{\substack{i,j \\ i<j}} (\mathbf{A}_{ij} - 1) \\
&= \frac{1}{e^{\sigma^2}-1} \left(S - \frac{K(K-1)}{2} \right)
\end{aligned} \qquad (67)$$

where, for notational convenience, we have defined $S \doteq \sum_{\substack{i,j \\ i<j}} \mathbf{A}_{ij}$. which in this case would be given by

$$S = \sum_{\substack{i,j \\ i<j}} e^{\sigma^2 p_b(d_{ij})} \qquad (68)$$

Finally, plugging (67) into (66) we arrive at

$$\mu_2 = \frac{(\log_2 10)^2}{100} K e^{2\mu+\sigma^2} \left(e^{\sigma^2} + \frac{2}{K}S \right) \qquad (69)$$

Now that the moments are available, the sum can be approximated by a log-normal random variable with location parameter M_{H} and scale parameter Ω given by

$$\begin{aligned}
\Omega^2 &= \log\left(\frac{\mu_2}{\mu_1^2} \right) \\
&= \log\left(e^{\sigma^2} + \frac{2}{K}S \right) - \log K
\end{aligned} \qquad (70)$$

$$\begin{aligned}
M_{\mathrm{H}} &= \log \mu_1 - \frac{1}{2}\Omega^2 \\
&= \mu + \frac{\sigma^2}{2} - \frac{1}{2}\log\left(e^{\sigma^2} + \frac{2}{K}S \right) \\
&\quad + \frac{3}{2}\log K + \log\left(\frac{\log_2 10}{10} \right)
\end{aligned} \qquad (71)$$

Finally, using $-Q^{-1}(x) = Q^{-1}(1-x)$, the outage capacity reads as

$$C_\epsilon^{\mathrm{H}} = C_{\mathrm{awgn}}^{\mathrm{H}} - e^{Q^{-1}(\epsilon)\Omega + M_{\mathrm{H}}} \qquad (72)$$

with $C_{\mathrm{awgn}}^{\mathrm{H}}$ given by (25) when K is large.

APPENDIX D
PROOF OF THEOREM 3

The approximation $\log_2(1+x) \approx x/\log 2$ applied to (30) yields $\mathrm{P}\left[\gamma\,\mathrm{trace}\left(\mathbf{D}^2\mathbf{B}^H\mathbf{B}\right)\log_2 e < C_\epsilon^{\mathrm{L}} \right] = \epsilon$. Let us define the random variable $\mathcal{I}_{\mathrm{L}} \triangleq \gamma\,\mathrm{trace}\left(\mathbf{D}^2\mathbf{B}^H\mathbf{B}\right)\log_2 e$, which is a sum of correlated random variables; if we approximate it with a Gaussian random variable, then the outage capacity reads as $C_\epsilon^{\mathrm{L}} = \sqrt{V_{\mathrm{L}}}Q^{-1}(1-\epsilon) + M_{\mathrm{L}}$, where M_{L} and V_{L} are the mean and variance of $\mathcal{I}_{\mathrm{L}}$, respectively.

The first value is easy to obtain, since $\mathbb{E}[\mathcal{I}_{\mathrm{L}}] = C_{\mathrm{low}}$ in (23) by definition. The second one is more involved; using the identity $\mathrm{var}[X] = \mathbb{E}[X^2] - \mathbb{E}[X]^2$, the binomial expansion (64), and the equality $\mathrm{trace}(\mathbf{D}^2\mathbf{B}^H\mathbf{B}) = \sum_{i=1}^{K} \delta_i^2 ||\mathbf{b}_i||^2$, we can write

$$\begin{aligned}
\mathrm{var}[\mathcal{I}_{\mathrm{L}}] &= (\log_2 e)^2 \gamma^2 \\
&\times \left(\mathbb{E}[\delta^4] \sum_{i=1}^{K} ||\mathbf{b}_k||^4 + 2 \sum_{\substack{i,j \\ i<j}} \mathbb{E}[\delta_i \delta_j] \cdot ||\mathbf{b}_i||^2 ||\mathbf{b}_j||^2 \right) \\
&\quad - C_{\mathrm{low}}^2.
\end{aligned} \qquad (73)$$

The value of $\mathbb{E}[\delta^4] = M_\delta(4)$ can be obtained from the approximation of the moments; on the other hand, the value of $\mathbb{E}[\delta_i \delta_j]$ has to be obtained by numerically solving the corresponding integral (38).

REFERENCES

[1] J. Arnau and C. Mosquera, "Performance analysis of multiuser detection for multibeam satellites under rain fading," in *Proc. ASMS & SPSC*, Baiona, Spain, Sep. 2012, pp. 197–204.
[2] A. Panagopoulos, P. D. M. Arapoglou, and P. Cottis, "Satellite communications at Ku, Ka, and V bands: Propagation impairments and mitigation techniques," *IEEE Commun. Surveys Tuts.*, vol. 6, no. 3, pp. 2–14, 2004.
[3] M. Filip and E. Vilar, "Optimum utilization of the channel capacity of a satellite link in the presence of amplitude scintillations and rain attenuation," *IEEE Trans. Commun.*, vol. 38, no. 11, pp. 1958–1965, 1990.

[4] J. Arnau, B. Devillers, C. Mosquera, and A. Perez-Neira, "Performance study of multiuser interference mitigation schemes for hybrid broadband multibeam satellite architectures," *EURASIP J. Wirel. Commun. Netw.*, vol. 2012, no. 1, p. 132, 2012.

[5] G. Zheng, S. Chatzinotas, and B. Ottersten, "Generic optimization of linear precoding in multibeam satellite systems," *IEEE Trans. Wireless Commun.*, vol. 11, no. 6, pp. 2308–2320, 2012.

[6] D. Christopoulos, S. Chatzinotas, G. Zheng, J. Grotz, and B. Ottersten, "Linear and nonlinear techniques for multibeam joint processing in satellite communications," *EURASIP J. Wirel. Commun. Netw.*, vol. 2012, no. 1, p. 162, 2012.

[7] J. Arnau-Yanez, M. Bergmann, E. Candreva, G. Corazza, R. de Gaudenzi, B. Devillers, W. Gappmair, F. Lombardo, C. Mosquera, A. Perez-Neira, I. Thibault, and A. Vanelli-Coralli, "Hybrid space-ground processing for high-capacity multi-beam satellite systems," in *Proc. IEEE Globecom*, Houton, TX., dec. 2011, pp. 1–6.

[8] D. Christopoulos, S. Chatzinotas, M. Matthaiou, and B. Ottersten, "Capacity analysis of multibeam joint decoding over composite satellite channels," in *Proc. ASILOMAR*, Pacific Grove, CA., 2011, pp. 1795–1799.

[9] D. Christopoulos, J. Arnau, S. Chatzinotas, C. Mosquera, and B. Ottersten, "MMSE performance analysis of generalized multibeam satellite channels," *IEEE Commun. Lett.*, vol. 17, no. 7, pp. 1332–1335, 2013.

[10] M. Castro and G. Granados, "Cross-layer packet scheduler design of a multibeam broadband satellite system with adaptive coding and modulation," *IEEE Trans. Wireless Commun.*, vol. 6, no. 1, pp. 248–258, jan. 2007.

[11] C. Kourogiorgas, A. Panagopoulos, and J. Kanellopoulos, "On the Earth-space site diversity modeling: novel physical-mathematical outage prediction model," *IEEE Trans. Antennas Propag.*, vol. 60, no. 9, pp. 4391–4397, 2012.

[12] A. Gharanjik, B. Rao, P.-D. Arapoglou, and B. Ottersten, "Gateway switching in Q/V band satellite feeder links," *IEEE Commun. Lett.*, vol. 17, no. 7, pp. 1384–1387, 2013.

[13] A. Kyrgiazos, B. Evans, P. Thompson, and N. Jeannin, "Gateway diversity scheme for a future broadband satellite system," in *Proc. ASMS & SPSC*, Baiona, Spain, Sep. 2012, pp. 363–370.

[14] K. Liolis, A. D. Panagopoulos, and P. Cottis, "Multi-satellite MIMO communications at Ku-band and above: investigations on spatial multiplexing for capacity improvement and selection diversity for interference mitigation," *EURASIP J. Wirel. Commun. Netw.*, vol. 2007, pp. 16–16, January 2007.

[15] V. Sakarellos, D. Skraparlis, A. Panagopoulos, and J. Kanellopoulos, "Outage performance analysis of a dual-hop radio relay system operating at frequencies above 10 GHz," *IEEE Trans. Commun.*, vol. 58, no. 11, pp. 3104–3109, 2010.

[16] K. Liolis, A. Panagopoulos, P. Cottis, and B. Rao, "On the applicability of MIMO principle to 10-66 GHz BFWA networks: capacity enhancement through spatial multiplexing and interference reduction through selection diversity," *IEEE Trans. Commun.*, vol. 57, no. 2, pp. 530–541, 2009.

[17] A. Panagopoulos, P. D. M. Arapoglou, G. Chatzarakis, J. Kanellopoulos, and P. Cottis, "LMDS diversity systems: a new performance model incorporating stratified rain," *IEEE Commun. Lett.*, vol. 9, no. 2, pp. 145–147, 2005.

[18] B. Gremont and M. Filip, "Spatio-temporal rain attenuation model for application to fade mitigation techniques," *IEEE Trans. Antennas Propag.*, vol. 52, no. 5, pp. 1245 – 1256, may 2004.

[19] N. Letzepis and A. Grant, "Capacity of the multiple spot beam satellite channel with rician fading," *IEEE Trans. Inf. Theory*, vol. 54, no. 11, pp. 5210 –5222, nov. 2008.

[20] A. Wyner, "Shannon-theoretic approach to a gaussian cellular multiple-access channel," *IEEE Trans. Inf. Theory*, vol. 40, no. 6, pp. 1713–1727, 1994.

[21] E. Lutz, M. Werner, and A. Jahn, *Satellite systems for personal and broadband communications*. Springer, 2000.

[22] C. Caini, G. Corazza, G. Falciasecca, M. Ruggieri, and F. Vatalaro, "A spectrum- and power-efficient EHF mobile satellite system to be integrated with terrestrial cellular systems," *IEEE J. Sel. Areas Commun.*, vol. 10, no. 8, pp. 1315–1325, 1992.

[23] R. M. Gray, "Toeplitz and circulant matrices: A review," *Foundations and Trends in Communications and Information Theory*, vol. 2, no. 3, 2005.

[24] ITU-R P.1853, "Tropospheric attenuation time series synthesis," Geneva, 2012.

[25] B. Holland and M. Ahsanullah, "Further results on a distribution of Meinhold and Singpurwalla," *The American Statistician*, vol. 43, no. 4, pp. 216–219, 1989.

[26] M. Abramowitz and I. A. Stegun, *Handbook of Mathematical Functions with Formulas, Graphs, and Mathematical Tables*. New York: Dover, 1964.

[27] L. Luini and C. Capsoni, "The impact of space and time averaging on the spatial correlation of rainfall," *Radio Science*, vol. 47, no. 3, 2012.

[28] ITU-R P.618-10, "Propagation data and prediction method required for the design of Earth-space telecommunication systems," Geneva, 2009.

[29] A. Ishimaru, S. Jaruwatanadilok, J. Ritcey, and Y. Kuga, "A MIMO propagation channel model in a random medium," *IEEE Trans. Antennas Propag.*, vol. 58, no. 1, pp. 178–186, 2010.

[30] D. Tse and P. Viswanath, *Fundamentals of wireless communication*. New York, USA: Cambridge University Press, 2005.

[31] I. Csiszár and J. Körner, *Information theory: coding theorems for discrete memoryless systems*, ser. Probability and mathematical statistics. Academic Press, 1981.

[32] M. Cheffena, L. Braten, and T. Ekman, "On the space-time variations of rain attenuation," *IEEE Trans. Antennas Propag.*, vol. 57, no. 6, pp. 1771–1782, june 2009.

[33] A. Papoulis and S. Pillai, *Probability, random variables, and stochastic processes*, 4th ed. McGraw-Hill, 2002.

[34] M. Lopez-Benitez and F. Casadevall, "Versatile, accurate, and analytically tractable approximation for the gaussian Q-function," *IEEE Trans. Commun.*, vol. 59, no. 4, pp. 917–922, 2011.

[35] O. Olabiyi and A. Annamalai, "Invertible exponential-type approximations for the gaussian probability integral $Q(x)$ with applications," *IEEE Wireless Commun. Lett.*, vol. 1, no. 5, pp. 544 –547, october 2012.

[36] N. Mehta, J. Wu, A. Molisch, and J. Zhang, "Approximating a sum of random variables with a lognormal," *IEEE Trans. Wireless Commun.*, vol. 6, no. 7, pp. 2690 –2699, july 2007.